

Please cite this article as:

M. Tedesco, E. Brauns, A. Cipollina, G. Micale, P. Modica, G. Russo, J. Helsen, Reverse Electrodialysis with saline waters and concentrated brines: a laboratory investigation towards technology scale-up, J. Memb. Sci. 492 (2015) 9–20.

<http://dx.doi.org/10.1016/j.memsci.2015.05.020>

Reverse Electrodialysis with saline waters and concentrated brines: a laboratory investigation towards technology scale-up

M. Tedesco^a, E. Brauns^b, A. Cipollina^{a*}, G. Micale^a, P. Modica^a, G. Russo^a, J. Helsen^{b§}

^aDipartimento di Ingegneria Chimica, Gestionale, Informatica, Meccanica, Università degli Studi di Palermo, Viale delle Scienze Ed.6, 90128 Palermo, Italy. *Corresponding author: andrea.cipollina@unipa.it, phone: +39 09123863718

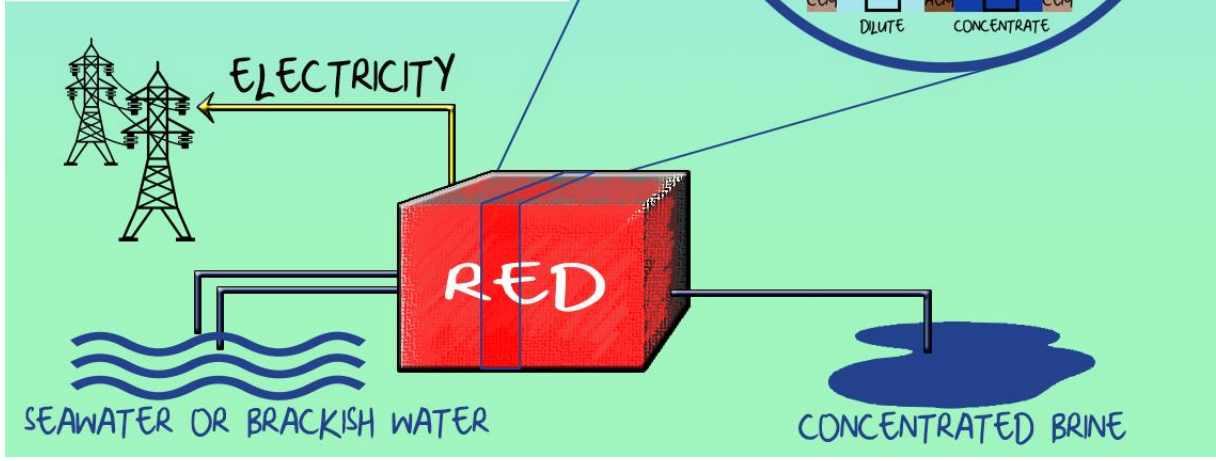
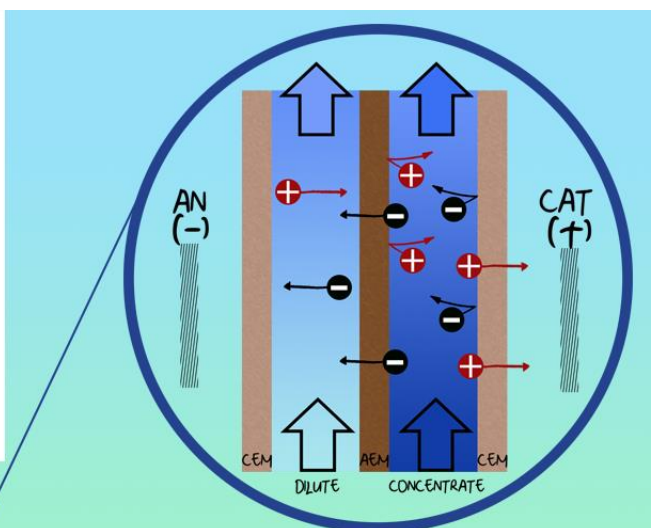
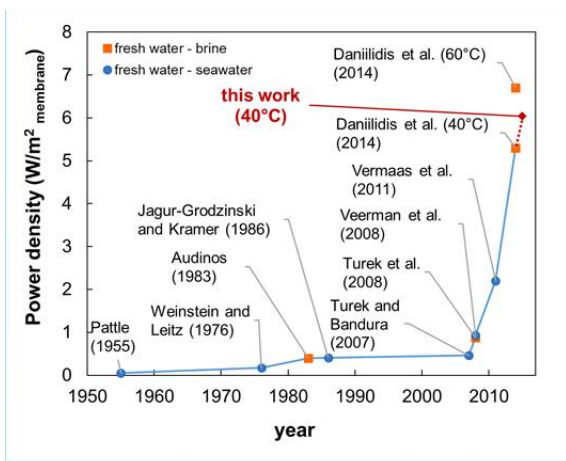
^bEnvironmental and Process Technology, VITO (Flemish Institute for Technological Research), Boeretang 200, B-2400, Mol, Belgium. §Corresponding author: joost.helsen@vito.be, phone: +32 14336940

Abstract

The use of concentrated brines and brackish water as feed solutions in reverse electrodialysis represents a valuable alternative to the use of river/sea water, allowing the enhancement of power output through the increase of driving force and reduction of internal stack resistance. Apart from a number of theoretical works, very few experimental investigations have been performed so far to explore this possibility.

In the present work, two RED units of different size were tested using artificial saline solutions. The effects of feed concentration, temperature and flowrate on process performance parameters were analysed, adopting two different sets of membranes. These experiments allowed to identify the most favourable conditions for maximising the power output within the presently investigated range, i.e. 0.1 M NaCl as diluate and 5 M NaCl as concentrate at 40°C. Under these conditions a power density equal to 12 W/m²_{cell_pair} was reached, among the highest so far reported in the literature. Increasing the unit size a slight reduction in power density was observed. These results indicate new directions for a successful scale-up and development of the Reverse Electrodialysis technology.

Keywords: salinity gradient power, RED, seawater, brackish water, brine



1 Introduction

Research activities on “water-related” renewable energy sources have increased during the last years. While hydroelectric processes already generate 800 GW worldwide, salinity gradient power (SGP) still remains an untapped source of green energy [1]. When two aqueous streams with different salinity (e.g. river water and seawater) are mixed together, an increase of entropy occurs, thus leading to a negative value of the Gibbs free energy of mixing. This amount of energy may well be harvested if a suitable controlled mixing process is carried out. A number of technologies have been proposed to convert SGP into mechanical energy [2] or electricity [3,4]. Among these, reverse electrodialysis (SGP-RE or RED) represents a promising technology, which could be easily commercialized as soon as new membranes will be available at competitive costs [5].

Within a reverse electrodialysis unit, cation and anion exchange membranes (AEMs and CEMs) are alternatively piled in a stack (Figure 1). Spacers (or profiled membranes [6]) are used to keep a proper distance between the membranes and create compartments for the feed solutions. During the operation, dilute (LOW) and concentrate (HIGH) solutions flow in alternate compartments. The concentration gradient leads to salt transport from the concentrate to the dilute compartments: these ion fluxes are regulated by the IEMs’ permselectivity, i.e. the selectivity towards cations (for CEMs) or anions (for AEMs). As a result, an ionic current is generated through the stack, and eventually converted into electric current by means of redox reaction at the electrodes.

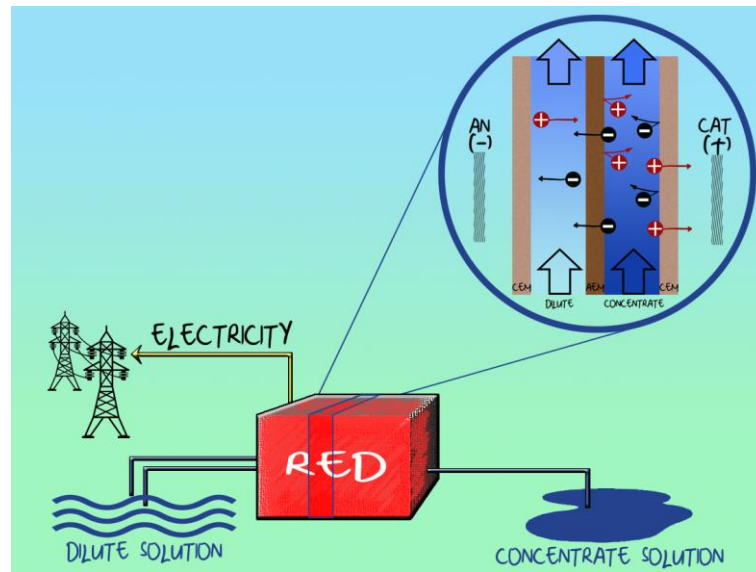


Figure 1. Principle of reverse electrodialysis (RED) process. The repeating unit of the system (*cell pair*) is constituted by a CEM, a concentrate compartment, an AEM and a dilute compartment.

The first experimental demonstration of the RED process dated back to 1955, when a power output of 15 mW (i.e. 0.05 W/m^2 of membrane) was reported by Pattle [7]. Conventional ED stacks, i.e. built with membranes and spacers commonly used for electrodialysis, were initially exploited for this purpose. In this way, a power density of 0.4 W/m^2 of membrane was achieved by Audinos in 1983, using a concentrated brine as concentrate feed solution [8]. However, the power obtainable from those early systems was limited by the lack of suitable ion exchange membranes [7–10].

The availability of new membranes and a deeper investigation on process conditions allowed to increase significantly the power produced by RED, especially during the last decade (Table 1). Among the works using artificial river water (0.017 M NaCl) and seawater (0.5 M NaCl) as

feed solutions, Veerman et al. obtained in 2008 a power density of 0.93 W/m² of membrane on a 50 cell pairs stack [11], being the maximum value achieved at that time. The work demonstrated that the use of low resistance membranes and a proper stack design (i.e. small compartments thickness, good sealing, etc.) are crucial aspects for enhancing the process performance.

Table 1. Literature works indicating the increasing trend of power density values experimentally obtained in RED systems.

year	Authors	Power density (W/m ² _{membrane})	spacer thickness and experimental conditions	Source
1955	Pattle	0.05	1 mm spacers, 39°C	[7]
1976	Weinstein and Leitz	0.17	1 mm spacers, 0.02 M – 0.57 M	[9]
1983	Audinos	0.40	1 mm spacers, 4.3 M	[8]
1986	Jagur-Grodzinski and Kramer	0.41	250 µm spacers, tap water and seawater	[10]
2007	Turek and Bandura	0.46	190 µm spacers, 0.01 M – 0.55 M	[12]
2008	Turek et al.	0.87	190 µm spacers, 0.01 M – 1.9 M	[13]
2008	Veerman et al.	0.93	200 µm spacers, 0.017 M – 0.5 M	[11]
2011	Vermaas et al.	2.20	60 µm spacers, 0.017 M – 0.5 M	[14]
2014	Daniilidis et al.	5.30	100 µm spacers, 0.01 M – 5 M, 40°C	[15]
2014	Daniilidis et al.	6.70	100 µm spacers, 0.01 M – 5 M, 60°C	[15]

Different electrode systems were tested, as the selection of suitable redox couple and electrodes also plays a role for improving the process performance, especially at laboratory-scale. The redox species commonly adopted for RED applications are iron redox couples, such as FeCl₃ / FeCl₂, K₃Fe(CN)₆/K₄Fe(CN)₆ and Fe(III)-EDTA/Fe(II)-EDTA. In particular, K₃Fe(CN)₆/K₄Fe(CN)₆ is widely used in RED laboratory investigations, thanks to its good stability in process conditions, provided that contact with oxygen and light is avoided [16]. The kinetics of electrochemical processes in such systems is generally controlled by mass transfer in the bulk solution, thus a concentration of the redox couple higher than 0.05 M is preferable to avoid high power losses [17].

Research efforts so far have been focused on two main directions for improvement: (i) reduction of stack resistance; (ii) enhancement of the generated electromotive force.

A reduction of the stack resistance has been obtained by using conductive spacers instead of common (uncharged) spacers. Długołęcki et al. in 2010 showed that the use of ion-conductive materials allows to halve the resistance when river water and seawater are used as feed, thus increasing the power density by a factor of 3 [18]. Starting from these results, further efforts have been focused on the construction of profiled membranes, where the spacers are substituted by properly structured IEMs. In this way, a reduction of the overall resistance was detected, yet resulting only into a slight increase of the power density due to a number of counteracting effects [6] likely to be attributed to the structure geometry, which is in fact not optimised for the process. Using pillar-structured membranes, Güler et al. in 2014 reached a 38% increase of power density (up to 1.3 W/m² of membrane) with respect to net-spacer equipped stack with flat membranes [19].

Although it is worth reducing the resistance of spacers and membranes, in most of literature works the largest contribution to the overall resistance was given by the diluate compartment, which was found to be up to 45% of the whole resistance when river water and seawater were used as feed solutions [11]. With this respect, the use of thinner compartments significantly

improves the process performance in such conditions. Following this strategy, a gross power density of 2.2 W/m^2 of membrane was reached by Vermaas et al. in 2011 using $60 \mu\text{m}$ spacers [14]. However, despite the significant improvement in the gross power output, the use of very thin spacer-filled channels cannot be suitable for practical applications, as it leads to very high pressure drops, dramatically affecting the value of net power output, and to an increasing risk of channel plugging.

On the other side, concerning the enhancement of salinity gradient and generated electromotive force, an interesting alternative to the use of seawater has been the choice of a feed stream with higher salinity such as concentrated brines. Of course, such non-conventional feed stream is limited to the availability of large amounts of brine, which is likely much less abundant than the conventional sources of sea and river water. However, a number of different scenarios can provide examples of sources of brines and bitterns with very high salt concentration, such as: concentrated brines from desalination plants, salt mines, saltworks or other industrial activities. The first experimental demonstration of this potential was given by Turek et al. in 2008, who reached 0.87 W/m^2 of membrane using fresh water (0.01 M NaCl) and coal-mine brine (1.9 M NaCl) [13]. More recently, Daniilidis et al. achieved a maximum power density of 5.3 W/m^2 with fresh water (0.01 M NaCl) and highly concentrated brine (5 M NaCl) at 40°C , using a small laboratory stack equipped with 5 cell pairs and thin spacers ($100 \mu\text{m}$) [15]. Moreover, increasing the temperature up to 60°C , a maximum power density of 6.7 W/m^2 of membrane was obtained by the same authors [15]. These conditions were identified after investigating a wider range of concentrations. However, this “optimal” dilute concentration dramatically depends on the membrane resistance and compartments thickness. In particular, when the system is characterised by large IEMs resistance or small compartment thickness, lower values of dilute feed concentration can lead to a beneficial increase in OCV, with a negligible increase of the overall stack resistance. At the contrary, adopting low resistance IEMs and thicker compartments would result in a dramatic effect of dilute concentration (especially in the range of very low concentrations) on the overall stack resistance, thus leading to the likely identification of different “optimal” conditions.

Finally, also in this case, the use of very thin compartments leads to unfavourable increases of pressure drops and pumping energy requirements.

On this basis, the use of brine in the concentrate compartment, combined with the use of brackish or sea water in the dilute one, can provide the operating conditions in a RED unit favourable to the enhancement of the generated electromotive force. Moreover, this choice can lead to the benefit of keeping a reduced stack resistance, even with realistically feasible compartment thicknesses, thus opening a large room for RED technology applications and process optimization [20–23].

This concept was demonstrated by theoretical analysis indicating how the use of brine and brackish water can have beneficial effects on the process performance, with optimal conditions dramatically depending on the stack size and geometry, solutions residence time and membrane features [24,25].

In the present work an extensive experimental campaign has been carried out using two reverse electrodialysis units fed with artificial saline waters and concentrated brines. In particular, two different sizes were tested: a (small) laboratory stack with $10 \times 10 \text{ cm}^2$ membrane area and 50 cell pairs, and a (large) scaled-up RED unit with $20 \times 20 \text{ cm}^2$ membrane area and 100 cell pairs, corresponding to an 8-folds increase in the stack membrane area. For the small stack, two different sets of membranes were tested. The dependencies of the process performance from the main operating conditions were analysed, such as concentration, flow velocity, and temperature of feed solutions. The investigated concentration and temperature ranges were

selected focusing on the real operating conditions for a pilot plant to be installed and operated with highly saline solutions in a real environment, while velocities were selected in order to get information on the suitable range allowing a positive net power output. This performance assessment allowed to identify the most feasible operating conditions for further scaling-up of the RED technology.

2 Experimental apparatus and procedures

The experimental campaign was performed at the Flemish Institute for Technological Research (VITO – Mol, Belgium) using a fully equipped test-rig. This section describes the experimental setup and procedure adopted during the tests.

2.1 Experimental apparatus

A fully automatized test-rig was built to monitor all the main operating variables (feed solutions flow rate, temperature, pressure, conductivity). The diluate (LOW) and the concentrate (HIGH) solutions are pumped to the RED unit from two tanks with a capacity of 200 liters each (Figure 2). Each tank is equipped with a stirrer and a temperature control system consisting of a heating and a cooling immersed coil.

Both LOW and HIGH circuits are equipped with two different pumps: (i) a centrifugal pump (Iwaki Magnet Pump 400CV5-D), with an automatic flow rate control; (ii) a peristaltic pump (Watson Marlow 604U) for tests at low flow rates.

The electrode rinse solution (ERS) is pumped to the stack from a 30 l tank using a peristaltic pump (Watson Marlow 604U). The ERS tank is also equipped with a stirrer (IKA RW 28) and a level control system. During the operation, all the transparent parts in the ERS circuit were covered with aluminium foil to avoid decomposition of the redox couple due to light exposure [16,26].

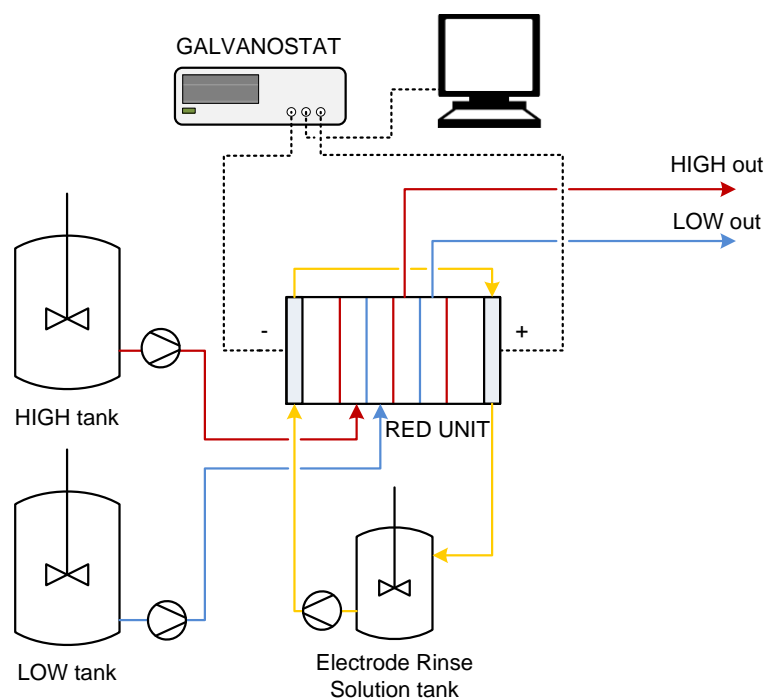


Figure 2. Simplified scheme of the experimental apparatus.

Conductivity meters (Mettler Toledo InPro 7100) and pressure transducers (Endress+Hauser Cerabar M) were installed at the inlet of each stream. A dedicated control software (MeFiAS[®])

was developed at VITO based on LabVIEW™ environment (National Instruments, USA). All the solutions' properties (flow rate, temperature, pressure, conductivity) for the three solutions and electric variables were monitored from the main panel of the software.

2.1.1 Reverse electrodialysis units

Two different RED units were tested for the experimental campaign: a first (small) unit with 10x10 cm² active membrane area equipped with 50 cell pairs, and a second (large) unit with 20x20 cm² active membrane area and 100 cell pairs (both stacks provided by REDstack BV, The Netherlands). Stacks were equipped with 270 μm polyamide woven spacers (Deukum GmbH, Germany). Two Ru-Ir oxide coated Ti electrodes were used in the end-compartments (Magneto Special Anodes BV, The Netherlands). A cross-flow arrangement was adopted for feeding solutions (Figure 3).

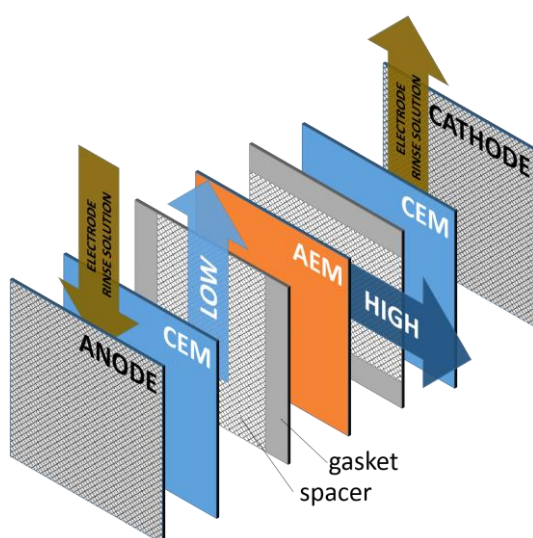


Figure 3. Description of cross-flow arrangement.

For the small RED unit, two different sets of ion-exchange membranes were used: a first set with thickness equal to 120 μm (thicker membranes), and a second set with thickness equal to 20 μm (thinner membranes), kindly supplied by Fujifilm Manufacturing Europe BV (The Netherlands) and FuMatech GmbH (Germany), respectively. Membrane properties are reported in Table 2.

It is worth noting that the use of thinner membranes has required special care to avoid their mechanical breakage and internal leakages. In particular, it was necessary to glue each membrane to the spacer's integrated gasket.

Table 2. Properties of the two sets of IEMs adopted in the experiments^a.

SET	Membrane	Thickness (μm)	Areal resistance ^b (Ω cm ²)	Permselectivity ^c (%)	Ion exchange capacity (meq/g)
1	Fujifilm AEM RP1 80045-01	120	1.83	96 %	1.28
	Fujifilm CEM RP1 80050-04	120	2.55	96 %	1.45
2	Fumasep FAS-20	20	0.5	95.5 %	1.50
	Fumasep FKS-20	20	1.7	99.02 %	1.24

^aData provided by membrane manufacturers.

^belectrical resistance measured in 0.5 M NaCl solution at 25°C.

^cpermselectivity measured in river water (0.017 M NaCl) – seawater (0.5 M NaCl) conditions.

Feed solutions were prepared using demineralised water and technical grade NaCl (ESCO, The Netherlands). The aqueous electrode rinse solution contained 0.1 M K₃Fe(CN)₆, 0.1 M K₄Fe(CN)₆ and 2.5 M NaCl as supporting electrolyte.

A reference test was defined (Table 3) fixing feed solutions concentration equal to seawater (0.5 M NaCl) and concentrated brine (5 M NaCl), a flow velocity of 1 cm/s and a temperature of 20°C. The dependencies on the main operating parameters (feed concentration, temperature, flow rates) were investigated changing one parameter per time.

Table 3. Conditions selected for the reference test.

Parameter	Reference test value
dilute concentration	0.5 M NaCl
concentrate concentration	5.0 M NaCl
fluid flow velocity	1.0 cm/s
temperature	20°C
<i>Electrode rinse solution properties:</i>	
composition	0.1 M K ₃ Fe(CN) ₆ , 0.1M K ₄ Fe(CN) ₆ , 2.5 M NaCl
conductivity	200 mS/cm
flow rate	30 l/h
temperature	20°C

2.2 Experimental procedures

2.2.1 Power density measurements

Power measurements tests were carried out in galvanostatic mode using a potentiostat/galvanostat (AMEL 2044), fully controlled by the MeFiAS[®] software developed on NI-Labview[™] platform. A current ramp in the range of 0 – 1 A was used, changing the current every 30 seconds with a step of 50 mA. The MeFiAS[®] software acquired the current (*I*) and stack voltage (*E_{stack}*) data during the experiment via respectively a Seneca T201DC100 and T201DC101 module with a frequency of 1 Hz. Therefore, the stack resistance can be calculated from Ohm's law:

$$E_{stack} = OCV - R_{stack} I \quad (1)$$

where OCV is the Open Circuit Voltage, and R_{stack} is the electrical resistance of the stack. The output power (P) is given by:

$$P = E_{stack} I \quad (2)$$

The power density is defined as the power generated per cell pair area:

$$P_d = \frac{P}{N A} \quad (3)$$

where N is the number of cell pairs and A is the area of one cell pair.

The net power density was estimated as the gross power output minus the theoretical pumping power required (assuming 100% pump efficiency), normalised by the total cell pair area of the stack:

$$P_{d,net} = \frac{P - \Delta p_{HIGH} Q_{HIGH}^{tot} - \Delta p_{LOW} Q_{LOW}^{tot}}{N A} \quad (4)$$

where Δp is the pressure drop inside the stack, Q^{tot} is the total flow rate, subscripts *HIGH* and *LOW* refer to concentrate and dilute stream, respectively.

Starting from the power output measurements, also gross and net yield were estimated, as the amount of energy generated from 1 m³ of feed solution. In particular, these were calculated as:

$$Y_{gross} = \frac{P}{Q_{LOW}^{tot}} \quad Y_{net} = \frac{P_{net}}{Q_{LOW}^{tot}} \quad (5, 6)$$

Where P and P_{net} are gross and the net power output, respectively, and Q_{LOW}^{tot} is the total volumetric flow rate of the dilute feed (equivalent to the volumetric flow rate of the concentrate feed in all tests presented in this work).

Finally, the energy efficiency can be estimated as the amount of produced power divided by the maximum theoretical power:

$$\eta = \frac{P}{P_{ideal}} \quad (7)$$

where the theoretical power is estimated from the Gibbs free energy of the mixing process:

$$P_{ideal} = 2RT Q^{tot} \left(C_{LOW} \ln \frac{\gamma_{LOW} C_{LOW}}{\gamma_{eq} C_{eq}} + C_{HIGH} \ln \frac{\gamma_{HIGH} C_{HIGH}}{\gamma_{eq} C_{eq}} \right) \quad (8)$$

where R is the universal gas constant, T is the absolute temperature and C_{eq} is the equilibrium concentration. The activity coefficients were estimated with the correlation proposed by Staples [27].

2.2.2 Evaluation of blank resistance and corrected power density

The amount of energy that can be harvested from a RED system is also affected by the active resistance of the electrode compartments, often known as blank resistance (R_{blank}). In a laboratory-scale unit, this contribution can be significant due to the relatively small number of cell pairs. However, when scaling-up to a stack with a large number of cell pairs (e.g. higher than 200), the power loss at the electrodes can be negligible [28]. Thus, in order to extrapolate the measured value of power density to the case of a stack where the effect of blank resistance is negligible, a correction procedure can be implemented to obtain the so-called ‘‘corrected Power density’’. This procedure is based on the measured value of OCV, overall stack resistance and blank resistance.

R_{blank} can be estimated by measuring experimentally the stack resistance at different number of cell pairs, plotting it and identifying the intercept of the regression line with the y-axis [28,29]. For this purpose, measurements were performed with 10, 30 and 50 cell pairs, and a blank resistance of 0.57Ω was estimated for the investigated conditions.

The total cell pairs resistance, R_{cells} can be calculated as:

$$R_{cells} = R_{stack} - R_{blank} \quad (9)$$

Therefore, a ‘‘corrected’’ stack voltage can be estimated by subtracting the voltage drops due to the cell pairs resistance from the OCV:

$$E_{stack,corr} = OCV - R_{cells} I_{corr} \quad (10)$$

where I_{corr} is the corrected current, equal to

$$I_{corr} = \frac{E_{stack,corr}}{R_u} \quad (11)$$

and R_u is the external load.

Substituting eq. (11) into eq. (10), gives

$$E_{stack,corr} = OCV - E_{stack,corr} \frac{R_{cells}}{R_u} \quad (12)$$

Rearranging eq. (12), and substituting into eqs. (2) and (3), the corrected power density ($P_{d,corr}$) is given by:

$$P_{d,corr} = \frac{OCV^2}{AR_u \left(1 + \frac{R_{cells}}{R_u}\right)^2} \quad (13)$$

Eq. (13) evaluates the corrected power density, representing an ideal unit where the blank resistance is equal to zero (i.e. a real unit with a very large number of cell pairs).

3 Results and discussion

The first part of the experimental campaign was focused on the effect of the main operating variables (concentration, velocity and temperature of the feed solutions) on process performance, testing the small RED unit ($10 \times 10 \text{ cm}^2$, 50 cell pairs) with two different sets of membranes. The investigated ranges were selected in order to fit the expected operative conditions of a pilot plant, which will be operating with saturated brine from saltworks basins (achieving saturation and temperatures up to $35\text{-}40^\circ\text{C}$) and lower concentration saline waters (i.e. brackish or sea water) [23]. The first set of membranes (Fujifilm- $120 \mu\text{m}$) was also adopted for analysing the effect of redox couple concentration on the power output.

Finally, after identifying for each variable the “best values” to maximise the power output, power density measurements at “best operating conditions” were performed aiming at the achievement of the maximum value of power output.

The larger RED unit ($20 \times 20 \text{ cm}^2$, 100 cell pairs), equipped with the thicker IEMs (Fujifilm- $120 \mu\text{m}$) was tested under similar operating conditions, though focusing only on the main dependencies on the diluate concentration and flow velocity.

A summary of experimental conditions for all tests is reported in Table 4.

Table 4. Summary of experimental tests presented in this work.

	IEMs set	Investigated variable	Investigated values
SMALL STACK ($10 \times 10 \text{ cm}^2$, $N = 50$)	Fujifilm $120 \mu\text{m}$	Flow velocity	$v = 0.5 - 4.0 \text{ cm/s}$
		Concentrate concentration	$C_{\text{HIGH}} = 1.0 - 5.0 \text{ M NaCl}$
		Diluate concentration*	$C_{\text{LOW}} = 0.1 - 1.0 \text{ M NaCl}$
		Feed temperature	$T = 20 - 40 \text{ }^\circ\text{C}$
		Redox couple concentration	$C_{\text{ELEC}} = 0.1 - 0.4 \text{ M}$
	Fumasep $20 \mu\text{m}$	Flow velocity	$v = 0.5 - 4.0 \text{ cm/s}$
		Diluate concentration	$C_{\text{LOW}} = 0.1 - 0.5 \text{ M NaCl}$
		Feed temperature	$T = 20 - 35 \text{ }^\circ\text{C}$
	Fujifilm $120 \mu\text{m}$	Best conditions	$C_{\text{HIGH}} = 5.0 \text{ M NaCl}$, $C_{\text{LOW}} = 0.1 \text{ M NaCl}$, $T = 40 \text{ }^\circ\text{C}$,
	Fumasep $20 \mu\text{m}$		$v = 2.0 \text{ and } 4.0 \text{ cm/s}$
LARGE STACK ($20 \times 20 \text{ cm}^2$, $N = 100$)	Fujifilm $120 \mu\text{m}$	Flow velocity	$v = 0.5 - 3.5 \text{ cm/s}$
		Diluate concentration	$C_{\text{LOW}} = 0.1 - 0.5 \text{ M NaCl}$
	Best conditions	$C_{\text{HIGH}} = 5.0 \text{ M NaCl}$, $C_{\text{LOW}} = 0.1 \text{ M NaCl}$, $T = 40 \text{ }^\circ\text{C}$,	
		$v = 1.0 - 3.0 \text{ cm/s}$	

* The effect of diluate feed concentration was further investigated between 0.01 and 0.1 M NaCl in separate tests presented in Figure 5.

3.1 Influence of feed solutions concentration

The effect of the feed solutions' concentration was assessed in two different sets of experiments, changing the HIGH and LOW concentration, alternatively.

The most remarkable effect has been observed for both sets of membranes when the diluate concentration (C_{LOW}) was varied. When lowering C_{LOW} and keeping C_{HIGH} constant, an increase in both the stack resistance and the Open Circuit Voltage is observed (Figure 4.A). These two effects have a counteracting influence on the power output, which is favoured by high OCV and low stack resistance. In the investigated range, a reduction of C_{LOW} always leads to higher power density, achieving at 0.1 M a maximum of about 4.5 W/m²_{cell pair} for the thicker membranes and of about 5.5 kWh/m²_{cellpair} for the thinner ones (Figure 4.B).

The measured values of OCV can be compared with the theoretical OCV calculated by the Nernst equation [24,30] assuming unitary permselectivity of IEMs (Figure 4.A). In particular, the theoretical OCV has been evaluated as

$$OCV^{(theoretical)} = 2N \frac{RT}{F} \ln \left(\frac{\gamma_{HIGH} m_{HIGH}}{\gamma_{LOW} m_{LOW}} \right) \quad (14)$$

where F is the Faraday constant, γ is the mean activity coefficient, m is the molal concentration; subscripts HIGH and LOW refer to concentrate and diluate, respectively.

The ratio between the measured and the theoretical membrane potential gives (by definition) the apparent permselectivity of IEMs [31]. Thus, the apparent permselectivity is equal to

$$\alpha = \frac{OCV^{(experimental)}}{OCV^{(theoretical)}} \quad (15)$$

Both the measured and the theoretical OCV are shown in Figure 4.A, while their ratio gives the average apparent permselectivity for each set of membranes.

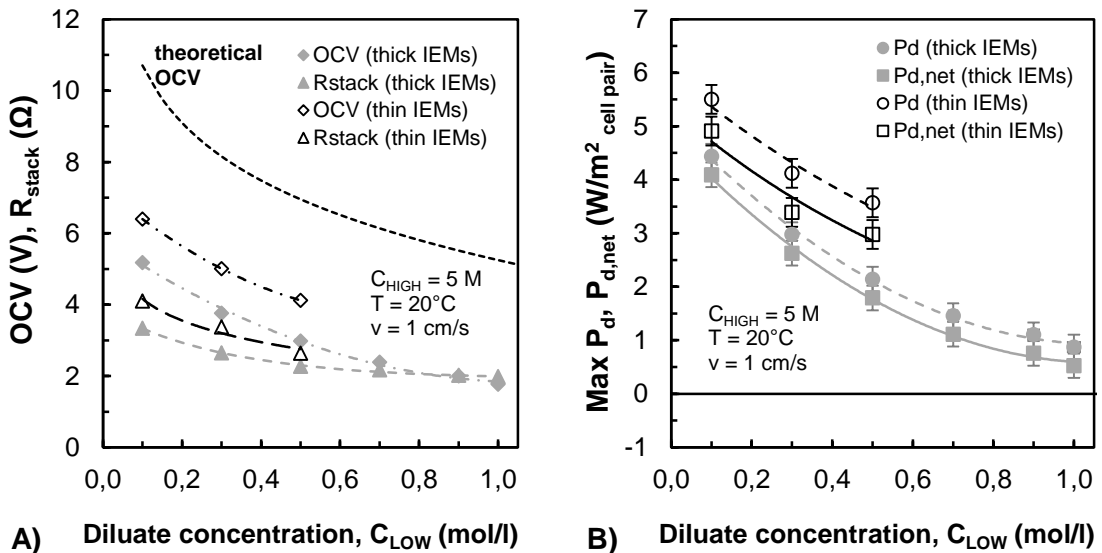


Figure 4. Influence of dilute solution concentration (C_{LOW}) on process performance. A) OCV and stack resistance. B) Net and gross power density. Experimental data for a 50 cell pairs stack equipped with 270 μm woven spacers, using thick IEMs (Fujifilm 120 μm), and thin IEMs (Fumasep 20 μm). $C_{HIGH} = 5 \text{ M}$; $T = 20^\circ\text{C}$, $v = 1 \text{ cm/s}$.

Higher OCV values are observed for thinner IEMs, thus indicating a better apparent permselectivity (around 0.6) compared to the thicker IEMs (around 0.4-0.5). This is in accordance with the IEMs specifications reported by suppliers for river water – seawater conditions (Table 2), though the presence of a highly concentrated brine dramatically reduces the actual permselectivity. On the other hand, the measurements resulted in a stack resistance larger for the set of thinner membranes (Figure 4.A). This is quite surprising, considering the expected effect of membranes thickness and also the nominal values of IEMs areal resistance (lower for the thinner membranes in river water – seawater conditions). This finding can likely be attributed to a different behaviour of the two membranes when in contact with highly concentrated solutions, which can generate swelling and ions sorption phenomena, affecting the ionic conductivity of the IEMs [32] and eventually leading to a lower actual resistance of the thicker membranes.

In order to extend the analysis beyond the selected experimental range and fit the conditions investigated also in previous literature works operating in a lower range of dilute salinity, the effect of dilute feed concentration (C_{LOW}) on the process performance was further investigated between 0.01 and 0.1 M NaCl. The tests were carried out at different flow velocities using only the thicker IEMs (Fujifilm 120 μ m). The results are reported in Figure 5.

Interestingly, a slight increase in power density is observed when the dilute concentration is below 0.1 M NaCl. However, below a critical value of concentration (0.04-0.06), a rapid reduction in the power output was registered. In particular, when operating the system at 0.01 M, no significant enhancement of the OCV is obtained (Figure 5.A), while such low concentration causes a notable increase on the stack resistance (Figure 5.B), leading to a drop of the power density well below the value previously obtained with a dilute concentration at 0.1M (Figure 5.C-D).

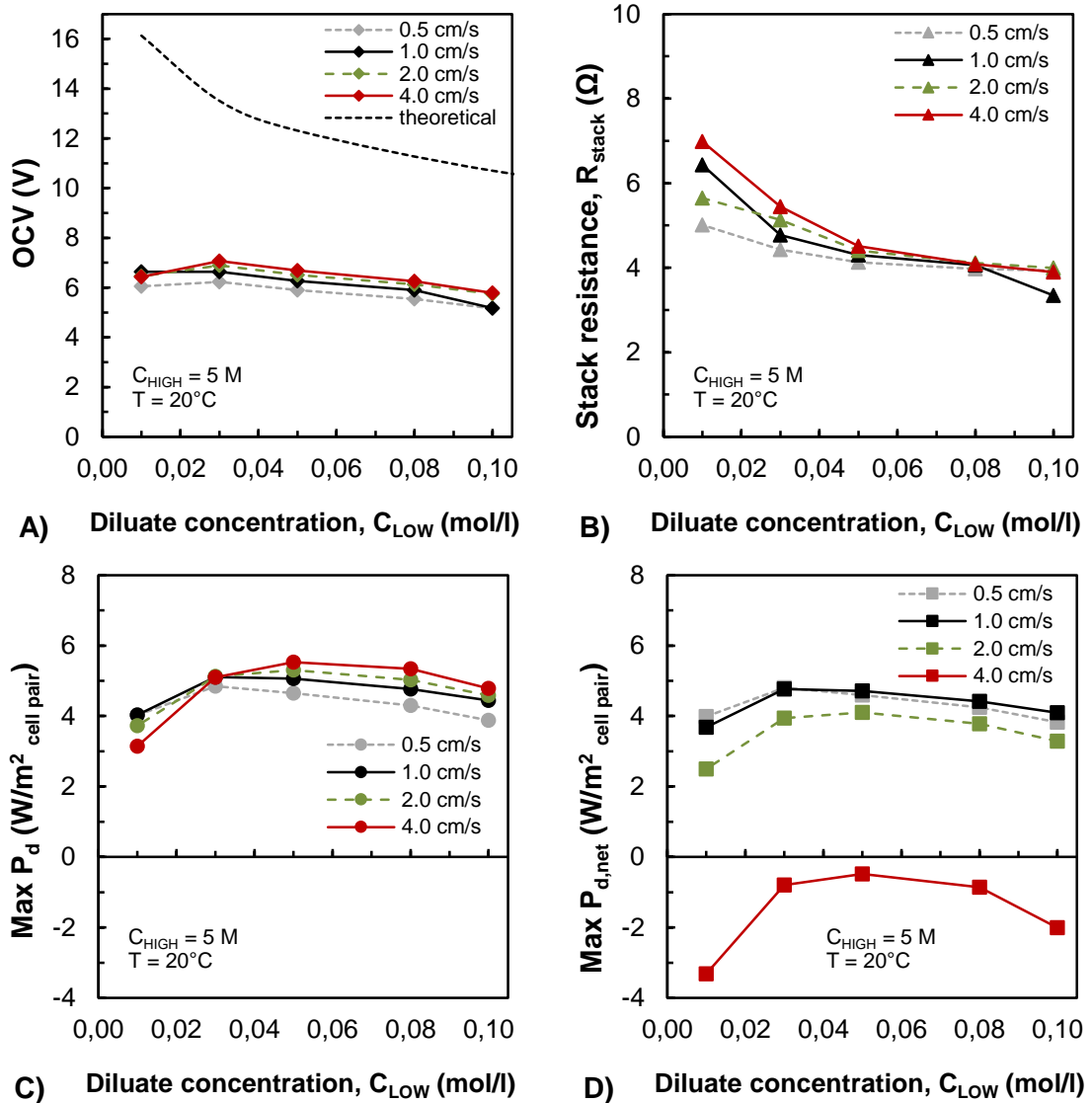


Figure 5. Influence of dilute solution concentration (C_{LOW}) on process performance in a lower range (0.01 – 0.1 M NaCl). A) OCV. B) Stack resistance. C) Gross power density. D) Net power density. Experimental data for a 50 cell pairs stack equipped with 270 μm woven spacers and thicker IEMs (Fujifilm 120 μm). $C_{HIGH} = 5$ M; $T = 20^\circ\text{C}$.

An optimal range of concentration can be identified between 0.03 and 0.08M for the present investigation. However, this can be dramatically dependent on a number of factors, i.e. stack geometry, membrane properties and flow velocity, as shown in Figure 5.

The effect of velocity on net power output is even more evident (Fig.5D), leading to negative values of the net power output when operating at 4 cm/s, as it will be better illustrated in the following paragraph.

The influence of brine concentration (C_{HIGH}) on OCV, R_{stack} and power density is reported Figure 6, for the case of thicker IEMs. As expected, the increase in C_{HIGH} from 1 M to 5 M NaCl leads to an increase in power density. This is due by the double beneficial effect of enhancing the process driving force (i.e. OCV) and reducing the stack resistance (Figure 6.A).

In particular, the maximum gross power density achieved at $C_{HIGH} = 5$ M, corresponding to the reference conditions test, is around $2 \text{ W/m}^2_{\text{cell pair}}$.

Figure 6.A also shows how increasing the HIGH concentration, a dramatic reduction in the mean apparent permselectivity from 0.8 to 0.4 is observed, due to the presence of the extremely concentrated brine in the system. This highlights how IEMs lose their permselectivity when in contact with very concentrated brines, as already reported in previous literature works [31,33].

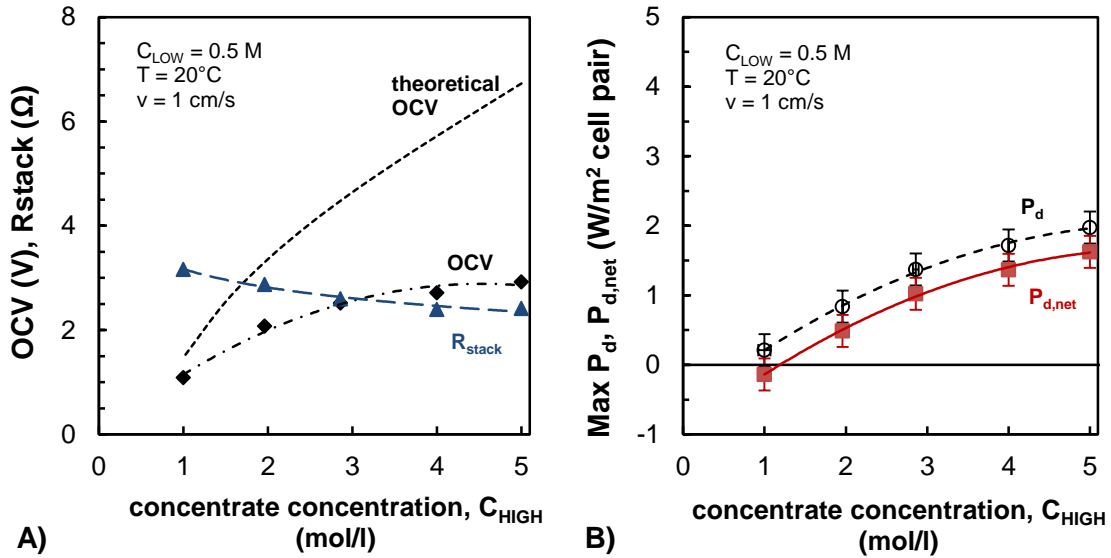


Figure 6. Influence of brine concentration (C_{HIGH}) on process performance. A) OCV and stack resistance. B) Net and gross power density. Experimental data for a 50 cell pairs stack equipped with Fujifilm ($120 \mu\text{m}$) membranes, $270 \mu\text{m}$ woven spacers. $C_{LOW} = 0.5 \text{ M}$; $T = 20^\circ\text{C}$, $v = 1 \text{ cm/s}$.

3.2 Influence of flow velocity

The flow velocity (v) has been defined as the mean fluid velocity inside a single spacer-filled channel. It can be estimated as:

$$v = \frac{Q}{\delta b \varepsilon_{sp}} \quad (16)$$

where Q is the volumetric flow rate (m^3/s) in a single channel, δ is the spacer thickness ($270 \cdot 10^{-6} \text{ m}$), b is the compartment width (0.1 m for the small stack) and ε_{sp} is the spacer porosity (82.5% for the woven spacer used in this study).

The influence of flow velocity was investigated in the range of $0.5 - 4 \text{ cm/s}$ for both diluate and concentrate (Figure 7), using $0.5 \text{ M} - 5 \text{ M}$ feed solutions at 20°C , with both sets of membranes. Figure 7.A reports the gross and net power density for both cases, while Figure 7.B shows both the energy efficiency and the yield, expressed as the amount of (gross and net) energy produced per cubic meter of feed solution.

In both cases, the increase in flow velocity slightly enhances the gross power density, achieving a value of about $4 \text{ W/m}^2_{\text{cell pair}}$ for the thinner IEMs and about $2 \text{ W/m}^2_{\text{cell pair}}$ for the thicker ones. Such trend is related to the reduction in the residence time, leading to a larger average salinity gradient between compartments, and the improvement of mixing phenomena inside compartments, although these latter play a minor role when seawater and brine are used [34].

For such highly saline solutions, the minor contribution of polarization phenomena and the resistance of the boundary layer have been also observed by EIS measurements [32].

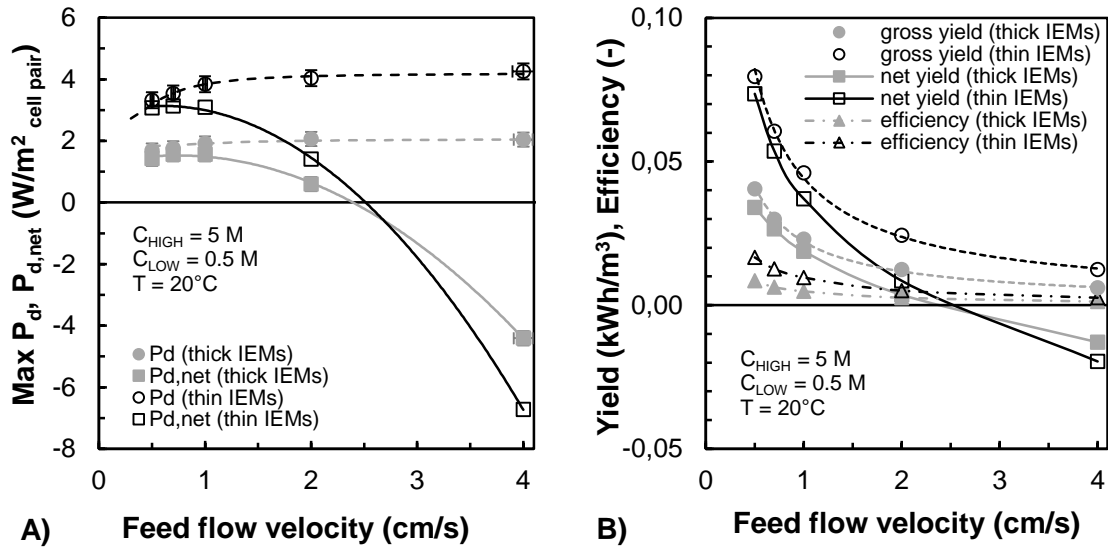


Figure 7. Effect of feed flow velocity on process performance. A) Gross and net power density. B) Efficiency and (gross and net) yield. Experimental data for a 50 cell pairs stack equipped with 270 μm woven spacers, using thick IEMs (Fujifilm 120 μm), and thin IEMs (Fumasep 20 μm). $C_{HIGH} = 5\text{ M}$; $C_{LOW} = 0.5\text{ M}$; $T = 20^\circ\text{C}$.

However, the most important influence of velocity is observed for the net power density and the yield. In fact, net power density decreases for flow velocities above 1 cm/s due to the significant increase in hydraulic losses. In particular, net power density becomes negative (i.e. the pumping power exceeding the gross power produced by the RED device) for flow velocities between 2 and 3 cm/s. A flow velocity between 0.5 and 1.0 cm/s was found to give a good balance between gross and net power output. Interestingly, though the same trend is observed for the two sets of membranes concerning the P_d , the use of thinner IEMs has led to a more pronounced reduction of the net power density, due to larger pressure drops generated by the glued stack assembly.

The yield of the process follows a monotonic decreasing trend when increasing velocity, with peak values of 0.04 kWh/m³ and 0.08 kWh/m³ achieved at 0.5 cm/s for thicker and thinner membranes, respectively. The corresponding values of energy efficiency are 0.8% and 1.7% for thicker and thinner membranes (Figure 7.B). Such low values can be attributed mainly to (1) short residence time; (2) low membrane permselectivity. The short residence time makes the outlet conditions of both solutions far from the equilibrium, thus recovering only a portion of the potential energy achievable. Indeed, higher flow velocity leads to a further reduction of the efficiency, reaching values below 1% when the flow velocity is higher than 2 cm/s. On the other side, the low membrane permselectivity due to the high salinity feed solutions leads to a lower recovery of the Gibbs free energy of mixing, since the passage of co-ions results in dissipative mixing without contributing to the RED power generation process. Conversely, higher energy efficiencies will be expected when the same membranes are used under conventional fresh water – seawater conditions.

As expected, using the thinner membranes, also a doubled yield was obtained compared to the use thicker ones, similarly to what observed for power density (Figure 7.B).

It is worth noting that at similar flow rates, a worst situation is expected in terms of net power output and net yield, when using very thin compartment. In fact, pressure drops depend on the cubic power of the spacer thickness, thus being dramatically enhanced by a reduction in channel

thickness. In practical applications, this would lead to unacceptable pressure drops already at relatively low velocities.

3.3 Influence of temperature

In order to assess the effect of temperature on the system, measurements were performed starting from the reference conditions (Table 3) and increasing the inlet temperature up to 40°C. A similar increase of power density has been observed (Figure 8) for the different membranes, ranging from 40% to 50% of the reference value. Such increase can be related to the strong dependence of membrane resistance on the system temperature, which can lead to a reduction between 30% and 50% when increasing the temperature from 20°C to 40°C [32].

The effect of temperature is also beneficial in increasing the conductivity of both solutions. However, in this case, relatively highly conductive solutions are used, and the main contribution to the stack resistance is due to the membranes: thus, the reduced stack resistance at higher temperature is likely due to the lower membrane resistance.

This result highlights the promising application of the RED process in locations where the temperature of feed streams are naturally high, e.g. when adopting brines from saltworks basins (typically at temperatures between 30°C and 40°C).

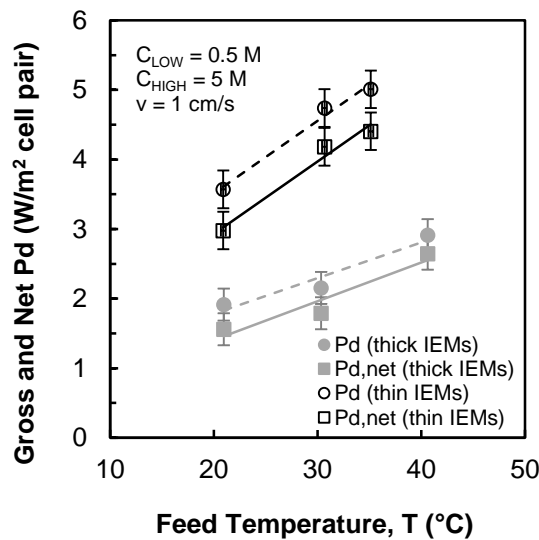


Figure 8. Influence of solutions temperature on the measured net and gross power density. Experimental data for a 50 cell pairs stack equipped with 270 μm woven spacers, using thick IEMs (Fujifilm 120 μm), and thin IEMs (Fumasep 20 μm). $C_{\text{HIGH}} = 5 \text{ M}$; $C_{\text{LOW}} = 0.5 \text{ M}$, $v = 1 \text{ cm/s}$.

3.4 Influence of redox couple concentration

As it concerns the effect of redox couple concentration, a focused analysis was performed using a stack equipped with the thicker IEMs, by varying redox couple concentration (C_{ELEC}) from 0.1 M (standard) to 0.4 M (Figure 9).

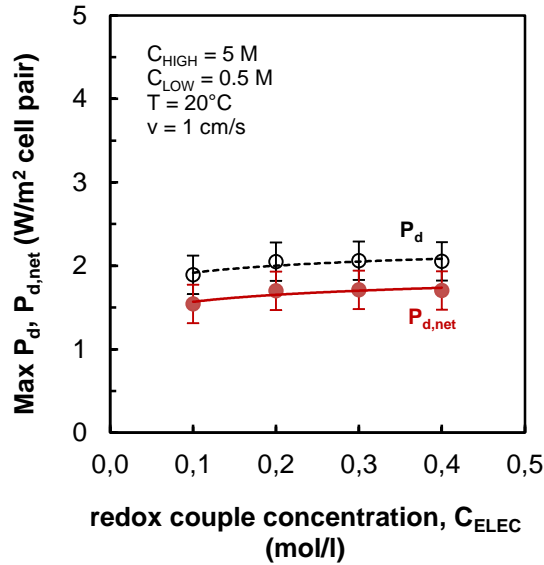


Figure 9. Influence of redox couple concentration in the electrode rinse solution on the measured net and gross power density. Experimental data for a 50 cell pairs stack equipped with Fujifilm (120 μ m) membranes, 270 μ m woven spacers. $C_{HIGH} = 5$ M; $C_{LOW} = 0.5$ M, $T = 20^\circ\text{C}$, $v = 1$ cm/s.

Figure 9 shows only a slight increase in power density passing from 0.1 M to 0.2 M, while beyond this point there is no significant effect of increasing the concentration. This may likely be related to the slight increase in electrodes redox reaction kinetics, reducing the blank resistance of the system.

However, such finding is not surprising, as the reference operating conditions for the electrode rinse solution (composition and flow rate) were selected in order to keep the mass flow rate within the electrodes compartments about 100 times larger than the reaction rate at the electrodes. Moreover, though electrode kinetics in RED units are often controlled by mass transfer phenomena, the use of redox species concentration above 0.05 M can normally avoid phenomena leading to limitations in the stack current density, at least in the investigated operating conditions [17].

3.5 Best conditions for maximum power production

Based on the aforementioned results, power density measurements were performed under the best conditions identified in the operating range defined in Table 4. In particular, the stacks equipped with both sets of membranes were tested using 0.1 M NaCl as dilute feed solution and 5 M NaCl as concentrate, an operating temperature of 40°C and a flow velocity fixed at 2.0 and 4.0 cm/s. The concentration of redox couple in the electrode rinse solution was set to 0.3 M. The measured values of power density are reported in Figure 10, along with the corrected power density (eq. 13), indicating the power output theoretically achievable by a stack with negligible blank resistance.

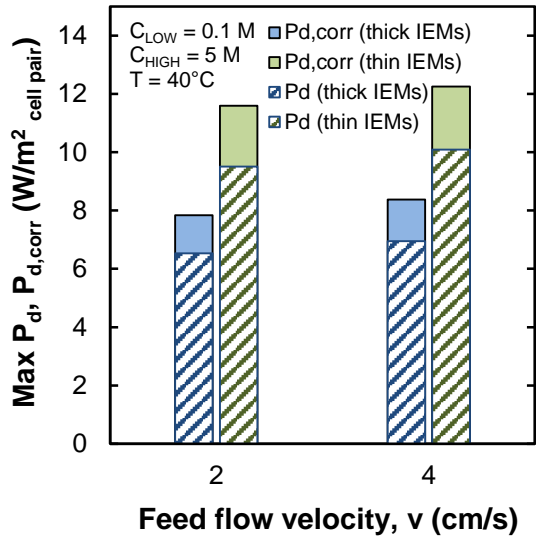


Figure 10. Power density under best operating conditions. Effect of feed flow velocity on power density (P_d) and corrected power density ($P_{d,corr}$). Experimental data for a 50 cell pairs stack equipped with 270 μm woven spacers, using thick IEMs (Fujifilm 120 μm) and thin IEMs (Fumasep 20 μm). $C_{HIGH} = 5 \text{ M}$; $C_{LOW} = 0.1 \text{ M}$; $T = 40^\circ\text{C}$. Redox couple concentration $C_{ELEC} = 0.3 \text{ M}$.

A power density around $6.5 \text{ W/m}^2_{\text{cell pair}}$ and $9.5 \text{ W/m}^2_{\text{cell pair}}$ was recorded for thick and thin membranes, respectively, with a negligible effect of flow velocity passing from 2.0 to 4.0 cm/s. Interestingly, a corrected power density of $8 \text{ W/m}^2_{\text{cell-pair}}$ was observed with the thicker membranes and $12 \text{ W/m}^2_{\text{cell-pair}}$ for thinner ones, corresponding to a value of 4 and 6 W/m^2 of membrane area, respectively.

Looking at the measured values of power density reported in the literature for reverse electro dialysis systems (Figure 11), these results constitute the highest values so far achieved when operating a RED unit at temperatures up to 40°C .

It is worth noting that, for comparison with literature data, Figure 10 and Figure 11 report only the gross power density. However, in the present case a net power density reduced by about $2\text{-}2.5 \text{ W/m}^2$ is registered at 2 cm/s and a practically null net power output is obtained at 4 cm/s. This is in substantial agreement with previous literature findings reporting also negative net power density values when exceeding a critical flow velocity (ranging from 1 to 3 cm/s, depending on the spacer thickness, channel geometry and operating conditions). A maximum value of net power density of $1.2 \text{ W/m}^2_{\text{membrane}}$ was reported by Veermas et al. in 2011 [14], obtained with a spacer thickness of 100 μm , an “empty-channel” velocity of slightly less than 1 cm/s and adopting river/sea water like feed solutions.

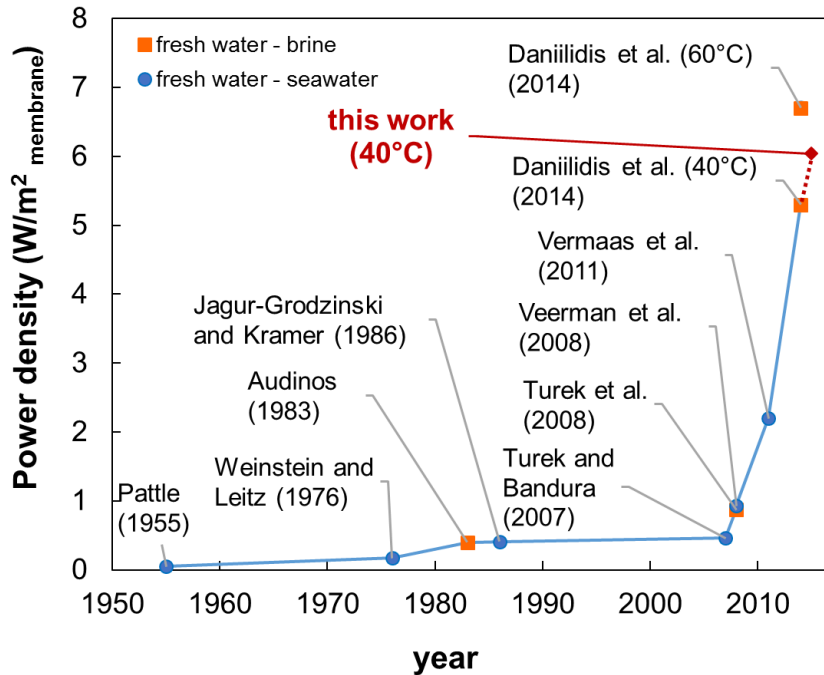


Figure 11. Historical trend of power density values (expressed as W/m^2_{membrane}) experimentally reported in RED technology literature. Blue circles refer to river/sea water conditions; orange squares refer to the use of brines and fresh water. The maximum value achieved in this work is reported as a red diamond for comparison with literature data. Sources: [7–15].

4 Towards technology scale-up: power measurements with a larger stack

In order to analyse the effects of RED process scale-up and provide preliminary information on the process scalability, a larger stack with $20 \times 20 \text{ cm}^2$ membrane area and 100 cell pairs (i.e. almost 10 times larger in terms of membrane area) was tested under similar experimental conditions of the smaller unit. The larger stack was equipped with Fujifilm 120-thick IEMs and $270 \mu\text{m}$ -thick woven spacers.

The influence of feed flow velocities on the gross and net power density is shown in Figure 12.A, using 0.5 M and 5 M NaCl solutions as diluate and concentrate, respectively. As a reference, also the results collected with the smaller RED unit are reported in the same graph. A clear reduction in power density is observed for the larger unit, likely related to (i) the doubled residence time within the scaled-up unit, leading to a loss in driving force (especially at lower velocities) and (ii) a difference in the stack-making, possibly leading to slightly different fluid dynamic conditions, parasitic currents in the manifolds and internal leakages, all aspects which is rather difficult to estimate quantitatively.

However, notwithstanding the lower power density achieved, the higher residence time for the larger stack has a beneficial effect on the system, resulting in a 40-50% increase in the gross yield (Figure 12.B). The net power density and energy efficiency followed a similar trend as the smaller stack, though a slightly lower threshold velocity between 1 and 2 cm/s was found, after which $P_{d,\text{net}}$ becomes negative.

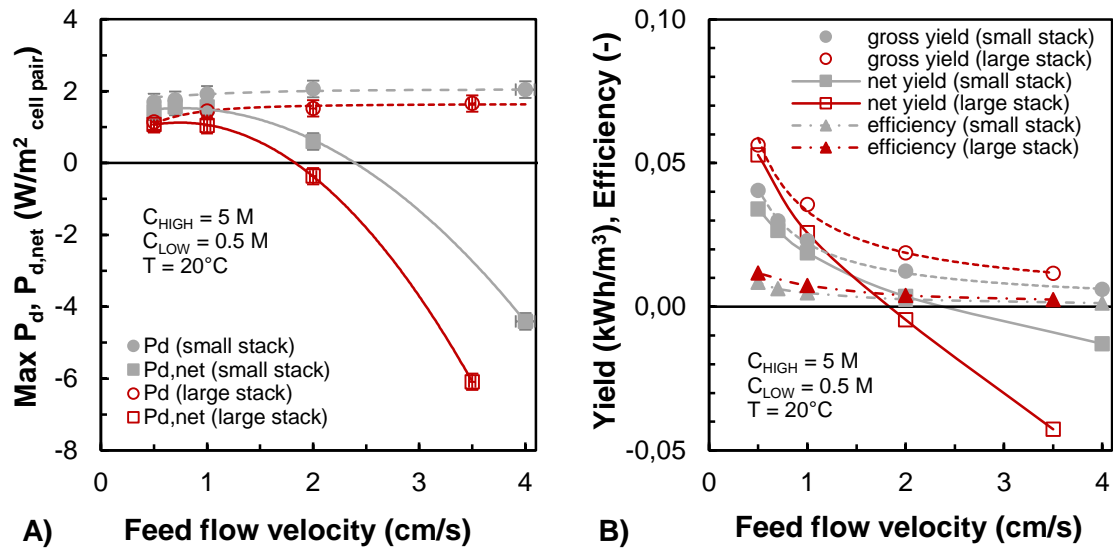


Figure 12. Effect of feed flow velocity on process performance for the small and large stack. A) Gross and net power density. B) Efficiency and (gross and net) yield. Small stack: $10 \times 10 \text{ cm}^2$, 50 cell pairs. Large stack: $20 \times 20 \text{ cm}^2$, 100 cell pairs. Both stacks equipped with $270 \text{ }\mu\text{m}$ woven spacers and thick IEMs (Fujifilm $120 \text{ }\mu\text{m}$). $C_{HIGH} = 5 \text{ M}$; $C_{LOW} = 0.5 \text{ M}$; $T = 20^\circ\text{C}$.

The effect of diluate concentration on the performance of both RED units is shown in Figure 13. Because of the doubled number of cell pairs in the larger stack, a 100% increase in the OCV values is observed (Figure 13.A). Such outcome suggests that any non-ideal phenomena that may reduce the OCV in scaled-up unit, such as parasitic currents in the manifolds [29], are not significant for the tested stacks.

Stack resistance is expected to be inversely proportional to the membrane area and directly proportional to the number of cell pairs (disregarding the contribution of the electrode compartments). As a consequence, the theoretical reduction of the stack resistance in the large unit should be expected equal to 50%. Conversely, only a 25% reduction has been experimentally observed (Figure 13.A). This could be related to a worse flow distribution within the larger stack, determining a non-uniform distribution of fluids concentration and velocity. Such discrepancy might also be due to a slightly larger resistance of the IEMs adopted in the large stack compared to those used in the smaller. In fact, the prototypal nature of the adopted IEMs, can lead to a lack of reproducibility of IEMs features themselves.

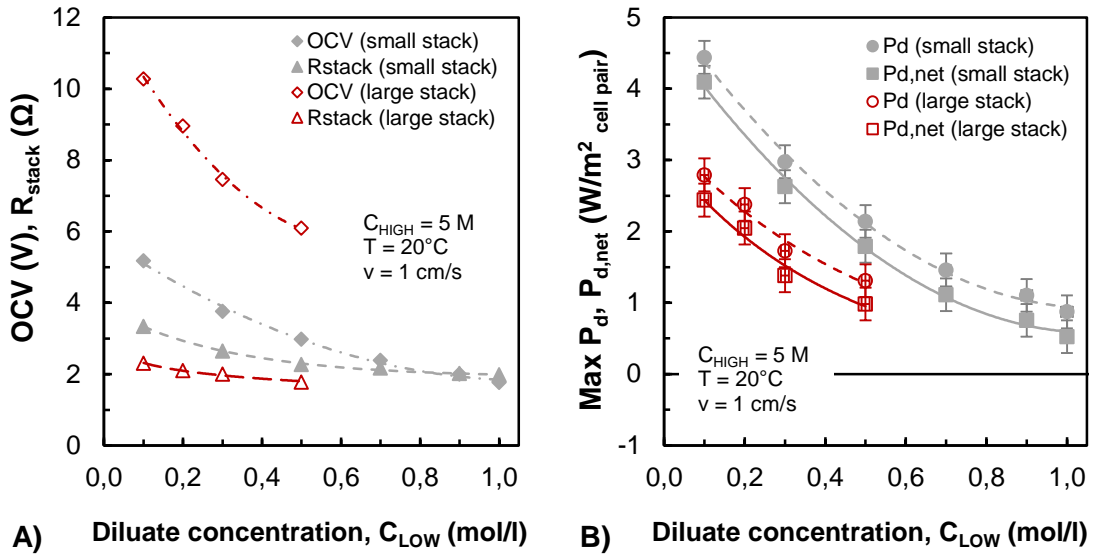


Figure 13. Effect of diluate concentration (C_{LOW}) on process performance at different scales. A) Gross and net power density. B) Gross and net efficiency. Small stack: $10 \times 10 \text{ cm}^2$, 50 cell pairs. Large stack: $20 \times 20 \text{ cm}^2$, 100 cell pairs. Both stacks equipped with $270 \text{ }\mu\text{m}$ woven spacers and thick IEMs (Fujifilm $120 \text{ }\mu\text{m}$). $C_{HIGH} = 5 \text{ M}$; $v = 1 \text{ cm/s}$; $T = 20^\circ\text{C}$.

In terms of power output, a smaller influence of diluate concentration is observed for the larger unit. An explanation of such behaviour can be related to the increased residence time in the larger unit, leading to a significant increase of the average concentration of the diluate, which smooth the sharper effect of C_{LOW} registered for the smaller unit.

Finally, the scaled-up unit was tested under the best conditions previously identified for the small RED unit. In particular, Figure 14 shows the power production obtained when the large stack was fed with 0.1 M NaCl and 5 M NaCl solutions at 40°C . Only a slight reduction in the obtainable power density is registered passing from the small to the larger stack, with a power density achieved slightly above $6 \text{ W/m}^2_{\text{cell pair}}$. When correcting the power density for taking into account the effect of blank resistance, only a 10% increase has been obtained, leading to a $P_{d,\text{corr}}$ between 6.6 and $6.8 \text{ W/m}^2_{\text{cell pair}}$. This demonstrates that, thanks to both the increased membrane area and the larger number of cell pairs, contributing to reduce the impact of R_{blank} on the overall stack resistance, for the large RED unit the “correction” of power density, is almost negligible as also indicated by previous analysis [28].

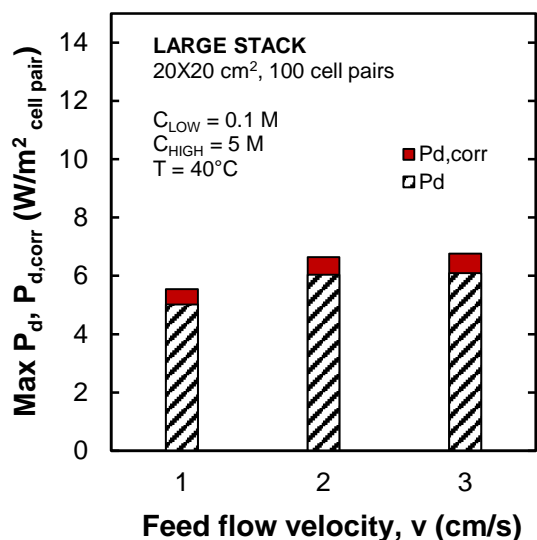


Figure 14. Investigation of best conditions for the scaled-up RED unit. Large stack: 20x20 cm², 100 cell pairs, equipped with 270 μm woven spacers and thick IEMs (Fujifilm 120 μm). C_{HIGH} = 5 M; C_{LOW} = 0.1 M; T = 40°C. Redox couple concentration C_{ELEC} = 0.3 M. A blank resistance of 0.14 Ω is considered for evaluating the corrected power density.

The results collected with the large RED unit demonstrate that an 8-fold increase of the membrane area does not lead to any appreciable loss of performance. In order to address the feasibility of the RED process for real applications, further investigations should be focused on (i) the use of natural solutions in real environments, (ii) process scale-up towards the industrial scale. With this regard, experimental works on laboratory scale with multivalent ions already highlighted that the performance of RED systems can be significantly reduced by the presence of Mg²⁺ [22,35]. A prototyping phase with natural solutions in real environment might be of paramount importance to assess the feasibility of process scale-up.

5 Conclusions

Focus of this work has been to investigate the effect of different membranes, stack size and operating conditions on the performance of reverse electro dialysis systems. Two RED units with different size were used: a small one, with 50 cell pairs of 10x10 cm² membrane area, and a large one, with 100 cell pairs of 20x20 cm² membrane area.

Results demonstrate how the increase in flow velocity can slightly increase the gross power output, however values above a critical velocity (2-3 cm/s for the investigated units and conditions) lead to unacceptable hydraulic pumping losses, even resulting into a negative net power output. Low fluid velocities are also beneficial in terms of process efficiency.

The choice of diluate feed concentration equal to 0.1 M NaCl (i.e. brackish water) can also be very beneficial in increasing power output and energy efficiency. Also the choice of increased feed temperature up to 40°C resulted in higher performances.

Most interestingly, when testing the system under the previously identified best operating conditions (i.e. 0.1 M NaCl and 5 M NaCl, 40°C and 2-4 cm/s flow velocity) a power density of about 8 W/m²_{cell pair} and 12 W/m²_{cell pair} was measured for the two different sets of IEMs. These are among the highest values of power density so far obtained in reverse electro dialysis systems.

Test runs with the 8-folds scaled-up unit resulted in similar dependences with respect to the monitored variables, though a slight reduction in power density was observed mainly due to an increase in the specific cell pair resistance.

Such findings are of paramount importance for the identification of the most favourable conditions in the design and construction of a pilot unit to be operated in a real environment and fed with saline waters and concentrated brines from natural saltworks.

Acknowledgments

This work has been performed within the REAPower (Reverse Electrodialysis Alternative Power production) project (www.reapower.eu), funded by the EU-FP7 programme (Project Number: 256736) within the Future Emerging Technologies topic.

The authors are also grateful to Fujifilm Manufacturing Europe BV and FuMa-tech GmbH for supplying the membranes adopted for the experimental campaign, and REDstack BV for providing the RED units.

Nomenclature

A	Active membrane area (m^2)
b	Membrane width (m)
C	Molar concentration (mol/l)
E_{stack}	Stack voltage (V)
$E_{stack,corr}$	Corrected stack voltage (V)
I	Electric current (I)
I_{corr}	Corrected electric current (I)
N	Number of cell pairs (-)
OCV	Open circuit voltage (V)
P	Power (W)
P_d	Power density (W/m^2 cell pair)
$P_{d,corr}$	Corrected power density (W/m^2 cell pair)
$P_{d,net}$	Net power density (W/m^2 cell pair)
P_{net}	Net power (W)
Q	Volumetric flow rate in a single channel (m^3/s)
Q_{tot}	Total feed volumetric flow rate (m^3/s)
R_{blank}	Blank resistance (Ω)
R_{cells}	Resistance of cell pairs pile (Ω)
R_{stack}	Stack resistance (Ω)
R_u	External load (Ω)
T	Temperature (K)
v	Fluid flow velocity (cm/s)

Greek letters

δ	Spacer thickness (μm)
Δp	Pressure drops (Pa)
ϵ_{sp}	Spacer porosity (%)
η_{gross}	Gross energy efficiency (-)
η_{net}	Net energy efficiency (-)

Subscripts

ELEC	Redox couple in the electrode rinse solution
HIGH	Concentrate solution
LOW	Dilute solution

Abbreviations

AEM	Anion exchange membrane
CEM	Cation exchange membrane
ERS	Electrode rinse solution
IEM	Ion exchange membrane
OCV	Open Circuit Voltage
RED	Reverse electrodialysis
SGP	Salinity gradient power

References

- [1] B.E. Logan, M. Elimelech, Membrane-based processes for sustainable power generation using water, *Nature*. 488 (2012) 313–319.
- [2] J.W. Post, J. Veerman, H.V.M. Hamelers, G.J.W. Euverink, S.J. Metz, K. Nijmeijer, et al., Salinity-gradient power: Evaluation of pressure-retarded osmosis and reverse electrodialysis, *J. Memb. Sci.* 288 (2007) 218–230. doi:10.1016/j.memsci.2006.11.018.
- [3] D. Brogioli, Extracting renewable energy from a salinity difference using a capacitor, *Phys. Rev. Lett.* 103 (2009) 058501(4).
- [4] B.B. Sales, M. Saakes, J.W. Post, C.J.N. Buisman, P.M. Biesheuvel, H.V.M. Hamelers, Direct power production from a water salinity difference in a membrane-modified supercapacitor flow cell, *Environ. Sci. Technol.* 44 (2010) 5661–5665.
- [5] A. Daniilidis, R. Herber, D.A. Vermaas, Upscale potential and financial feasibility of a reverse electrodialysis power plant, *Appl. Energy*. 119 (2014) 257–265. doi:http://dx.doi.org/10.1016/j.apenergy.2013.12.066.
- [6] D.A.A. Vermaas, M. Saakes, K. Nijmeijer, Power generation using profiled membranes in reverse electrodialysis, *J. Memb. Sci.* 385–386 (2011) 234–242. doi:10.1016/j.memsci.2011.09.043.
- [7] R.E. Pattle, Production of Electric Power by mixing Fresh and Salt Water in the Hydroelectric Pile, *Nature*. 174 (1954) 660.
- [8] R. Audinos, Inverse Electrodialysis. Study of Electric Energy Obtained Starting with Two Solutions of Different Salinity, *J. Power Sources*. 10 (1983) 203–217.
- [9] J.N. Weinstein, F.B. Leitz, Electric power from differences in salinity: the dialytic battery, *Sci. (New York, NY)*. 191 (1976) 557.
- [10] J. Jagur-Grodzinski, R. Kramer, Novel process for direct conversion of free energy of mixing into electric power, *Ind. Eng. Chem. Process Des. Dev.* 25 (1986) 443–449.
- [11] J. Veerman, M. Saakes, S.J. Metz, G.J. Harmsen, Reverse electrodialysis: Performance of a stack with 50 cells on the mixing of sea and river water, *J. Memb. Sci.* 327 (2009) 136–144. doi:10.1016/j.memsci.2008.11.015.
- [12] M. Turek, B. Bandura, Renewable energy by reverse electrodialysis, *Desalination*. 205 (2007) 67–74.
- [13] M. Turek, B. Bandura, P. Dydo, Power production from coal-mine brine utilizing reversed electrodialysis, *Desalination*. 221 (2008) 462–466.
- [14] D.A.A. Vermaas, M. Saakes, K. Nijmeijer, Doubled Power Density from Salinity Gradients at Reduced Intermembrane Distance, *Environ. Sci. Technol.* 45 (2011) 7089–7095. doi:10.1021/es2012758.

- [15] A. Daniilidis, D.A.A. Vermaas, R. Herber, K. Nijmeijer, Experimentally obtainable energy from mixing river water, seawater or brines with reverse electrodialysis, *Renew. Energy*. 64 (2014) 123–131. doi:<http://dx.doi.org/10.1016/j.renene.2013.11.001>.
- [16] O. Scialdone, C. Guarisco, S. Grispo, A.D. Angelo, A. Galia, Investigation of electrode material - Redox couple systems for reverse electrodialysis processes. Part I: Iron redox couples, *J. Electroanal. Chem.* 681 (2012) 66–75.
- [17] O.S. Burheim, F. Seland, J.G. Pharoah, S. Kjelstrup, Improved electrode systems for reverse electro-dialysis and electro-dialysis, *Desalination*. 285 (2012) 147–152. doi:[10.1016/j.desal.2011.09.048](http://dx.doi.org/10.1016/j.desal.2011.09.048).
- [18] P. Długołęcki, J. Dabrowska, K. Nijmeijer, M. Wessling, Ion conductive spacers for increased power generation in reverse electrodialysis, *J. Memb. Sci.* 347 (2010) 101–107.
- [19] E. Güler, R. Elizen, M. Saakes, K. Nijmeijer, Micro-structured membranes for electricity generation by reverse electrodialysis, *J. Memb. Sci.* 458 (2014) 136–148. doi:<http://dx.doi.org/10.1016/j.memsci.2014.01.060>.
- [20] E. Brauns, Towards a worldwide sustainable and simultaneous large-scale production of renewable energy and potable water through salinity gradient power by combining reversed electrodialysis and solar power?, *Desalination*. 219 (2008) 312–323. doi:[10.1016/j.desal.2007.04.056](http://dx.doi.org/10.1016/j.desal.2007.04.056).
- [21] A. Cipollina, A. Misseri, G.D. Staiti, A. Galia, G. Micale, O. Scialdone, Integrated production of fresh water, sea salt and magnesium from sea water, *Desalin. Water Treat.* 49 (2012) 390–403.
- [22] R.A. Tufa, E. Curcio, W. Van Baak, J. Veerman, S. Grasman, E. Fontananova, et al., Potential of brackish water and brine for energy generation by salinity gradient power-reverse electrodialysis (SGP-RE), *RSC Adv.* 4 (2014) 42617–42623.
- [23] M. Tedesco, A. Cipollina, A. Tamburini, G. Micale, J. Helsen, M. Papapetrou, REAPower: use of desalination brine for power production through reverse electrodialysis, *Desalin. Water Treat.* 53 (2015) 3161–3169. doi:[10.1080/19443994.2014.934102](http://dx.doi.org/10.1080/19443994.2014.934102).
- [24] M. Tedesco, A. Cipollina, A. Tamburini, I.D.L. Bogle, G. Micale, A simulation tool for analysis and design of reverse electrodialysis using concentrated brines, *Chem. Eng. Res. Des.* 93 (2015) 441–456. doi:[10.1016/j.cherd.2014.05.009](http://dx.doi.org/10.1016/j.cherd.2014.05.009).
- [25] M. Tedesco, P. Mazzola, A. Tamburini, G. Micale, I.D.L. Bogle, M. Papapetrou, et al., Analysis and simulation of scale-up potentials in reverse electrodialysis, *Desalin. Water Treat.* Doi [10.1080/19443994.2014.947781](http://dx.doi.org/10.1080/19443994.2014.947781).
- [26] O. Scialdone, A. Albanese, A.D. Angelo, A. Galia, C. Guarisco, Investigation of electrode material - Redox couple systems for reverse electrodialysis processes. Part II: Experiments in a stack with 10–50 cell pairs, *J. Electroanal. Chem.* 704 (2013) 1–9. doi:<http://dx.doi.org/10.1016/j.jelechem.2013.06.001>.

- [27] B.R. Staples, Activity and Osmotic Coefficients of Aqueous Alkali Metal Nitrites, *J. Phys. Chem. Ref. Data.* 10 (1981) 765–777.
- [28] M. Tedesco, A. Cipollina, A. Tamburini, W. van Baak, G. Micale, Modelling the Reverse ElectroDialysis process with seawater and concentrated brines, *Desalin. Water Treat.* 49 (2012) 404–424.
- [29] J. Veerman, J.W. Post, M. Saakes, S.J. Metz, G.J. Harmsen, Reducing power losses caused by ionic shortcut currents in reverse electroDialysis stacks by a validated model, *J. Memb. Sci.* 310 (2008) 418–430. doi:10.1016/j.memsci.2007.11.032.
- [30] N. Lakshminarayanaiah, Transport phenomena in artificial membranes, *Chem. Rev.* 65 (1965) 491.
- [31] H. Strathmann, Ion-exchange membrane separation processes, Elsevier Science Limited, 2004.
- [32] E. Fontananova, W. Zhang, I. Nicotera, C. Simari, W. Van Baak, G. Di Profio, et al., Probing membrane and interface properties in concentrated electrolyte solutions, *J. Memb. Sci.* 459 (2014) 177–189. doi:http://dx.doi.org/10.1016/j.memsci.2014.01.057.
- [33] K. Kontturi, L. Murtomäki, J.A. Manzanares, Ionic Transport Processes: In *Electrochemistry and Membrane Science*, OUP Oxford, 2008.
- [34] L. Gurreri, A. Tamburini, A. Cipollina, G. Micale, M. Ciofalo, CFD prediction of concentration polarization phenomena in spacer-filled channels for reverse electroDialysis, *J. Memb. Sci.* 468 (2014) 133–148. doi:http://dx.doi.org/10.1016/j.memsci.2014.05.058.
- [35] D.A. Vermaas, J. Veerman, M. Saakes, K. Nijmeijer, Influence of multivalent ions on renewable energy generation in reverse electroDialysis, *Energy Environ. Sci.* 7 (2014) 1434–1445.